Anti-phase synchronization in microelectromechanical systems and effect of impulsive perturbations

Qingfei Chen,[1] Ying-Cheng Lai,[1,2,3] Junseok Chae,[1] and Younghae Do[3]
[1]*School of Electrical, Computer, and Energy Engineering, Arizona State University, Tempe, Arizona 85287, USA*
[2]*Department of Physics, Arizona State University, Tempe, Arizona 85287, USA*
[3]*Department of Mathematics, Kyungpook National University, Daegu, 702-701, South Korea*
(Received 24 January 2013; published 9 April 2013)

We show that anti-phase synchronization can emerge in a pair of electrically coupled micromechanical beams. Under impulsive perturbation, desynchronization occurs, distorting the output of each beam. We derive a formula for the relaxation rate and verify it numerically. We also find that the difference between the displacements of the two beams, or the differential signal, is robustly immune to impulsive perturbation, implying that the system can effectively counter external disturbances. This can have significant applications in the development of various microscale devices, which we elaborate on using microelectromechanical resonators.

DOI: 10.1103/PhysRevB.87.144304 PACS number(s): 05.45.Xt, 05.45.Pq, 85.85.+j

I. INTRODUCTION

Synchronization is a universal phenomenon in a variety of natural and engineering systems.[1,2] In recent years, interest in synchronization in micro- or nanoscale systems has emerged,[3–10] motivated by the potential that synchronization can be exploited for significant applications in nanoscience and nanotechnology. In this regard, phase locking in a pair of mechanically coupled nanobeams was demonstrated.[6] Quite recently, the idea of using optical coupling to synchronize micromechanical oscillators has been exploited[9,10] for potential application in realizing massive optomechanical oscillator arrays.[11,12]

In this paper, we articulate a class of electrically coupled, micromechanical oscillator systems and show that anti-phase synchronization can arise in such a system. Our system consists of a pair of nearly identical micromechanical beams driven by a differential electrical signal as shown in Fig. 1 where the traditional, extremely widely used SMS is also shown for comparison. Let $u_+(x,t)$ and $u_-(x,t)$ be the displacements of the two beams, respectively. The anti-phase synchronization state[13] is defined by $u_+(x,t)+u_-(x,t)=0$. We develop a realistic model, incorporating multiple physical effects, such as beam bending, fluid-pressure forces, and electrostatic force. One particularly interesting issue concerns the consequence of impulsive perturbation which, in reality, can be mechanical shocks, a sudden drop of the device, or disturbances from extreme operational environments. When the system is perturbed in such a fashion, synchronization will be destroyed temporally, but the system can relax to the anti-phase synchronous state after a certain amount of time. We obtain a theoretical formula for the relaxation rate and verify it numerically. An interesting finding is that the *differential displacement* between the two beams, defined by $\bar{u}(x,t)=u_+(x,t)-u_-(x,t)$, depends on the electrical driving but is *extremely insensitive* to impulsive perturbation, regardless of whether anti-phase synchronization is achieved. This implies that our electrically coupled, double-beam, or differential configuration represents a novel class of microelectromechanical (MEM) systems with superior capability to counter impulsive perturbation. We note that developing effective strategies to mitigate such perturbation in MEM systems is a problem of tremendous engineering and technological interest.[14–19] Thus, our work and finding not only contribute to the basic nonlinear dynamics of microscale systems, but also have the potential to lead to effective shock-immune MEM systems for a variety of significant, state-of-the-art technological applications.

In Sec. II, we describe the detailed physical model of our coupled MEM system. In Sec. III, we analyze the relaxation dynamics to anti-phase synchronization and argue that the differential signal is robust against impulsive perturbation. In Sec. IV, we present an application example to design robust MEM resonators. A brief summary is presented in Sec. V.

II. MODEL OF AN ELECTRICALLY COUPLED MEM SYSTEM

A physically detailed model of a pair of electrically coupled MEM beams consists of four components: equations of motion, electrostatic force equation, squeeze-film damping formulation (fluid-pressure forces), and impulsive perturbation. Without loss of generality, we consider the case of doubly clamped MEM beams (similar considerations apply to other MEM configurations, such as cantilevers or circular plates).

Equations of motion. Applying the classical Euler-Bernoulli theory to both beams with constant cross-sectional area, we obtain the following equation of motion:

$$\rho A_\pm \frac{\partial^2 u_\pm}{\partial t^2} + EI_\pm \frac{\partial^4 u_\pm}{\partial x^4} = F_\pm^E + F_\pm^A + F_\pm^S, \qquad (1)$$

where both beams are along the x axis at rest, $u_\pm$'s denote the beam deflections in the z direction, ρ is the material density, $A_\pm = w_\pm \delta_\pm$ is the area (width × thickness; we assume $w_\pm \equiv w$ and $\delta_\pm \equiv \delta$), and $I_\pm = w\delta^3/12$ is the moment of inertia of the two beams' cross sections, $F_\pm^E$ is the electrostatic forces per unit length, $F_\pm^A$ is the fluid-pressure forces, and $F_\pm^S$ is the external impulsive forces acting on the beams. The fluid-pressure forces are given by

$$|F_\pm^A| = \int_{-w/2}^{w/2} |p_\pm(x,y) - P_{am}| dy,$$

where $p_\pm$ is the interior air pressure acting on beams "+" and "−," respectively, and P_{am} is the ambient air pressure outside the volume of the two parallel beams. When the squeeze-film effect is present and if the beams are not at rest, we have

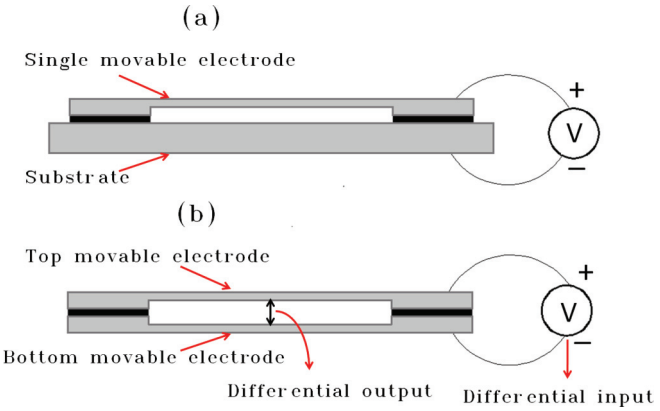

FIG. 1. (Color online) (a) Traditional single movable structure (SMS) in electrostatically actuated MEM systems where a single micromovable electrode is suspended over a fixed electrode. A voltage is applied between them. (b) Our scheme of a pair of parallel movable electrodes where a differential voltage input signal is applied to both beams.

$p_\pm \neq P_{am}$. In Eq. (1), we assume that the deflections of the beams are small, a common situation for realistic MEM devices. In this case, the residual stresses in the fixed beam system can be neglected. The boundary conditions at the two fixed ends of both beams are

$$\begin{aligned} u_\pm(0,t) = u_\pm(L,t) = 0, \\ \partial u_\pm(0,t)/\partial t = \partial u_\pm(L,t)/\partial t = 0. \end{aligned} \tag{2}$$

Electrostatic force. When the MEM system is in operation so that the beams are bent, the capacitance of the differential beam system depends on the deflection geometry of the beams and so does the electrostatic force. The capacitance of the differential MEM capacitors can be approximated by that due to a number of small capacitors in parallel. Neglecting deflection along the y direction, for a certain value of x and a small length dx, the capacitance is given by

$$C(x) = \frac{\epsilon_0 w\, dx}{Z(x)},$$

where $Z(x) = Z_0 + u_+(x) - u_-(x)$ is the gap distance between the two beams at position x, Z_0 is the initial gap between the two parallel beams, ϵ_0 is the dielectric constant of the medium, and nonhomogeneity in the charge distribution has been neglected due to movement of the beams. The potential energy associated with the small capacitance is $E(x) = C(x)V^2/2$. The electrostatic forces per unit length on the two beams are given by $F^E_\pm = (1/dx)[dE(x)/du_\pm]$. Because of the fringing-field effect in the parallel-plate configuration, small corrections to the electrostatic forces on the two beams are necessary,[20] which can be modeled by the following correctional coefficient to the force expressions: $(1 + 0.65Z/w)$. Taking this effect into account, the resulting electrostatic forces can be expressed as

$$F^E_+ = -\frac{\epsilon_0 w V^2}{2Z^2(x)}\left[1 + 0.65\frac{Z(x)}{w}\right] = -F^E_-. \tag{3}$$

Fluid-pressure forces. Under the assumption that the deflections of the two beams are small, the beam system can be regarded as a series of moving pairs of plates of length dx and gap $Z(x)$. When the space in between a pair of moving plates is filled with gas or fluid, a squeezed-film effect can arise.[21,22] In particular, when the plates move in the direction perpendicular to the gas film, the following two phenomena can occur: (1) The pressure inside the gas changes due to the plate motion, and (2) gas can be either squeezed out or sucked in from the edge of the plate surfaces. The pressure distribution in the gap $Z(x)$ can be modeled by the classical Reynolds equation,

$$12\eta\frac{\partial(pZ)}{\partial t} = \nabla[(1 + 6k_n)Z^3 p\nabla p], \tag{4}$$

where $p = p(x,y)$, η is the viscosity of the fluid, k_n is the Knudsen number given by $k_n = k_b T/(2\pi P_{am} d^2 Z)$, T is the absolute temperature, and d is the collision diameter of the fluid molecules. Under room temperature, the value of k_n is usually small and can be neglected. In addition, the pressure gradient in the z direction is negligible. Equation (4), thus, reduces to

$$12\eta\frac{\partial Z}{\partial t} = \frac{\partial}{\partial x}\left(Z^3\frac{\partial p}{\partial x}\right) + \frac{\partial}{\partial y}\left(Z^3\frac{\partial p}{\partial y}\right), \tag{5}$$

which is linear in p so that the pressure can be replaced by the difference between the internal pressure of the fluid and that of the ambient $\tilde{p} = p - P_{am}$. Applying the boundary condition $\tilde{p} = 0$ to the beam edges and using the assumption that the pressure is a separable function of x and y, i.e., $\tilde{p}(x,y,t) = \tilde{P}(x,t)(1 - 4y^2/w^2)$, we obtain

$$12\eta\frac{\partial \hat{Z}}{\partial t} = 2\hat{Z}^2\left(\frac{Z_0}{L}\right)^2\frac{\partial \hat{Z}}{\partial \hat{x}}\frac{\partial \tilde{P}}{\partial \hat{x}} + \frac{2}{3}\hat{Z}^3\left(\frac{Z_0}{L}\right)^2\frac{\partial^2 \tilde{P}}{\partial \hat{x}^2} - 8\frac{\hat{Z}^3}{\hat{w}^2}\tilde{P}, \tag{6}$$

where $Z = Z(x,t)$ is assumed to be independent of y and the following nondimensionalized quantities are used: $\hat{x} = x/L$ (L: beam length), $\hat{Z} = Z/Z_0$, and $\hat{w} = w/Z_0$. Since, generally, we have $Z_0 \ll L$ for a doubly clamped MEM beam, Eq. (6) can be further simplified by dropping terms on the order of $(Z_0/L)^2$. The pressure can, thus, be obtained as $\tilde{P}(x,t) = (3/2)(\eta w^2/Z^3)(\partial Z/\partial t)$. Since the pressure gradient in the gas film is assumed to be negligible, the fluid pressure on the two capacitors is equal in magnitude $[p_+(x,y) = p_-(x,y) = p(x,y)]$, but the resulting forces are opposite to each other. The two fluid-pressure forces per unit length F^A_+ and F^A_- are, thus, given by

$$\begin{aligned} F^A_+ &= \int_{-w/2}^{w/2}[p_+(x,y) - P_{am}]dy = \int_{-w/2}^{w/2}[p(x,y) - P_{am}]dy \\ &= \int_{-w/2}^{w/2}\tilde{p}dy = \int_{-w/2}^{w/2}\tilde{P}(x,t)\left(1 - \frac{4y^2}{w^2}\right)dy = \frac{\eta w^3}{Z^3}\frac{\partial Z}{\partial t}, \end{aligned} \tag{7}$$

$$\begin{aligned} F^A_- &= \int_{-w/2}^{w/2}[P_{am} - p_-(x,y)]dy \\ &= \int_{-w/2}^{w/2}[P_{am} - p(x,y)]dy = -\int_{-w/2}^{w/2}\tilde{p}\,dy \\ &= -\int_{-w/2}^{w/2}\tilde{P}(x,t)\left(1 - \frac{4y^2}{w^2}\right)dy = -\frac{\eta w^3}{Z^3}\frac{\partial Z}{\partial t}. \end{aligned} \tag{8}$$

Force due to impulsive perturbation. In realistic MEM devices, a mechanical shock load is transmitted from the supports (e.g., package or wafer) to the microstructure. Due to the small size of the MEM system, the forces can be regarded equivalently as the distributed acceleration pulls over the microstructure. The load on the two beams can be regarded as identical due to their symmetry. The impulsive force per unit length can, thus, be modeled as $F_+^S(x,t) = F_-^S(x,t) = \alpha\rho w h(t)$, where α is the pulse amplitude and $h(t)$ is the pulse profile over time. To be concrete, we will use the rectangular profile for impulsive force perturbation.

III. RELAXATION TO ANTI-PHASE SYNCHRONIZATION AND ROBUSTNESS AGAINST IMPULSIVE PERTURBATION

When impulsive perturbation is absent, the double-beam MEM system exhibits an anti-phase synchronization state defined by $u_+ + u_- = 0$. When such a perturbation is applied, synchronization is destroyed. After the perturbation, the system typically goes through a relaxation process towards synchronization. The rate of relaxation is important and is key to the performance of the MEM system in response to impulsive perturbation. The leading damping force in the device is that due to the squeeze-film damping, but since the directions along which they act on the two beams are opposite to each other, they have little effect on synchronization. As a result, otherwise insignificant damping forces, such as the linear viscous force of the moving beam and the thermal-elastic damping force,[23] will dominate the relaxation dynamics. That is, these forces will be significant particularly near the anti-phase synchronization manifold $\hat{u}$ where fluid forces are approximately canceled. Taking into account the linear viscous and thermal-elastic damping forces, we obtain the following dynamical equation:

$$\rho A\frac{\partial^2 u_\pm}{\partial t^2} - b\frac{\partial u_\pm}{\partial t} + EI\frac{\partial^4 u_\pm}{\partial x^4} = F_\pm^A + F_\pm^E + F_\pm^S, \quad (9)$$

where b is the damping coefficient. Focusing on the dynamical variable $\hat{u} = u_+ + u_-$, which characterizes the dynamics of the beam system in the subspace transverse to the anti-phase synchronization manifold, we get

$$\rho A\frac{\partial^2 \hat{u}}{\partial t^2} - b\frac{\partial \hat{u}}{\partial t} + EI\frac{\partial^4 \hat{u}}{\partial x^4} = 2F^S, \quad (10)$$

which is the equation of motion of a single beam under a mechanical load in a damping environment. From Eq. (10), we can see that, when impulsive perturbations are present, the anti-phase synchronization state is no longer a solution. To calculate the relaxation rate, we set $F^S = 0$ so that $\hat{u} = 0$ is a solution of the system. Note that Eq. (10) has the form of a single free-motion beam system under dissipation. The relaxation rate at which $\hat{u} \to 0$ can then be measured as the rate $R(t)$ of the energy loss of a free-motion beam system described by Eq. (10) for $F^S = 0$. For solutions corresponding to harmonic oscillations, since the two parallel beams have the same resonant frequency, we can set $\hat{u}(x,t) = \hat{u}_0(x)\exp(i\omega t)$, where ω is complex, its real part $\mathrm{Re}(\omega)$ gives the new eigenfrequencies of the beam in the damping environment, and the imaginary part $\mathrm{Im}(\omega)$ characterizes attenuation of the oscillation, which is the energy-loss rate. Substituting this form of $\hat{u}(x,t)$ into Eq. (10) for $F^S = 0$ and collecting the coefficients of $\exp(i\omega t)$, we get

$$EI(d^4\hat{u}_0/dx^4) - ib\omega\hat{u}_0 - \rho A\omega^2\hat{u}_0 = 0.$$

The normal modes of oscillation of the beam[24] are described by

$$\hat{u}_0(x) = C_1\sin(qx) + C_2\cos(qx) + C_3\sinh(qx) + C_4\cosh(qx),$$

where $C_{1\text{–}4}$ are the coefficients of different modes. A simple substitution then gives $EIq^4 - ib\omega - \rho A\omega^2 = 0$, which leads to $\omega = (ib + \sqrt{4\rho AEIq^4 - b})(2\rho A)$. The energy-loss rate is given by

$$R = 2\,\mathrm{Im}(\omega) = \frac{b}{\rho A}. \quad (11)$$

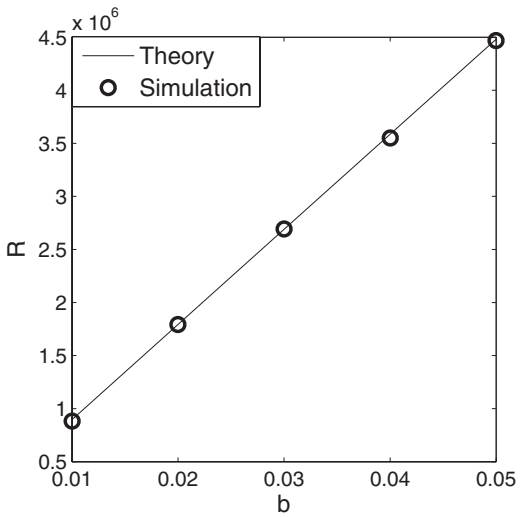

FIG. 2. Energy-loss rate versus the damping coefficient where the solid line represents the theoretical prediction Eq. (11) and the open circles are numerical data.

Figure 2 shows the simulation results of R from Eq. (10) in comparison with the theoretical predictions Eq. (11). The structural parameters are $L = 80$, $w = 5$, and $\delta = 1$ μm. In the numerical computation, a rectangular impulsive force of strength $a = 500$ g is applied to the system from $t = 0$ to $t = 0.1$ s, and the decay rate of the peak amplitude of the oscillation is measured: $R_e = -2\ln[\hat{u}(t_2)/\hat{u}(t_1)]/(t_2 - t_1)$, where t_1 and t_2 ($t_2 > t_1$) are the occurrence times of the first two peaks of $\hat{u}(t)$. We observe an excellent agreement between theory and numerics.

After an impulsive perturbation, the more symmetrical the system is, the faster $\hat{u}$ relaxes to 0, leading to more desirable dynamics of the differential system. To enhance the relaxation rate, one can change the design of the beam structure, e.g., by adjusting the cross-sectional area A, to make the decay $\hat{u}(t) = \hat{u}(t_0)\exp[-(R/2)(t - t_0)]$ faster. It is, however, difficult to control the damping parameter b. Consider, for example, a MEM resonator, which is typically designed to work in a low-pressure environment where b is near zero so as to increase the signal-to-noise ratio. In such a case, when an impulsive perturbation occurs, the anti-phase synchronization

state and the desired motion of each microbeam will be strongly perturbed within a certain time, leading to a significant signal-integrity issue if the resonator was of the SMS type. By the merit of our differential MEM scheme, the impulsive perturbation will not affect the desired differential beam motion, despite the lack of anti-phase synchronization.

We now present the general principle for applications of our differential MEM system in countering impulsive perturbation. To contrast, we will compare its performance against such perturbation with that associated with the traditional SMS MEM systems widely used in all kinds of modern technologies. The basic observation is that the perturbation effects on the two beams can cancel each other but not the electrical signals. In particular, a closer examination of Eq. (1) and the force expressions reveals that the two beams are, in fact, coupled through the dynamical variable $Z(x)$. Due to symmetry, the electrostatic forces acting on them are equal in magnitude but opposite in sign and, so, are the fluid-pressure forces. Another distinctive feature of Eq. (1) is that, whereas, the whole system is nonlinear, the nonlinearity originates solely from the force terms $F_{\pm}^{E}$ and $F_{\pm}^{A}$, which are valid when the deflections of the beams are relatively small. The spatiotemporal evolution of the differential signal $\bar{u} = u_{+} - u_{-}$ is, thus, governed by

$$\rho A \frac{\partial^2 \bar{u}}{\partial t^2} + EI \frac{\partial^4 \bar{u}}{\partial x^4} = 2 \frac{w \epsilon V^2}{2(Z_0 - \bar{u})^2} \left(1 + 0.65 \frac{Z_0 - \bar{u}}{w}\right) + 2 \frac{\eta w^3}{(Z_0 - \bar{u})^3} \frac{\partial \bar{u}}{\partial t}. \quad (12)$$

The consequences of Eq. (12) are the following. First, $\bar{u}(x,t)$ represents a low-dimensional manifold of the differential MEM system, meaning that the dynamics of $\bar{u}$ are independent of those of $u_{\pm}$. Second, the underlying system is on the scale of a micron, so any realistic mechanical disturbances to the two beams can be regarded as identical. As a result, the impulsive perturbation forces on the two beams do not appear in Eq. (12), indicating that such forces effectively cancel each other in the manifold. Third, the dynamics of $\bar{u}(x,t)$ in the manifold has the same form as that of the dynamics of a single electrostatic MEM beam. This is so because the first and second terms on the right-hand side of Eq. (12) are mathematically identical to two times the corresponding terms for the electrostatic force and the squeezed-film damping force in an SMS system. To make up for the factor of 2 in these two forces, we can design the system so that the fluid viscosity is increased by the same factor and the required driving voltage is reduced by the factor of $\sqrt{2}$. This way, the intrinsic dynamics of the MEM beam system are retained, but the external impulsive disturbances are effectively eliminated. Except for these parameter changes, there is no need to alter the design principles with respect to specific performance criteria. In addition, the required voltage can be smaller as compared with that associated with the conventional SMS beam-electrode configuration. This can help mitigate common problems in applications of MEM switches, such as a high-voltage drive.[25]

IV. APPLICATION EXAMPLE: MEM RESONATORS

To give a concrete application example, we focus on an important class of devices: MEM resonators and carry out systematic finite-element simulations. To be realistic, we take into account two types of mismatches: damping and beam thickness mismatches and compare the main performance characteristics with those of an SMS MEM resonator.

In general, our differential MEM setting is compatible with the widely used MEM capacitive-sensing principle,[26,27] which can be seen as follows. The traditional configuration of a capacitive MEM actuator consists of a movable electrode and a fixed electrode parallel to it. A voltage is applied between the movable and the fixed electrodes, creating an electrostatic force that tends to drag the movable electrode downwards. In the differential setting shown in Fig. 1(b), the output signal is taken as the relative displacement between the electrodes: $\bar{u} = u_{+} - u_{-}$, where $u_{\pm}$ are the displacements of the upper and lower ones. The displacement signal from an oscillating beam system can be sensed by some standard measurement circuit.[28] In our design, for resonator applications, the two parallel beams also act as a measurement device for converting relative displacement into electric current. In particular, the oscillations of the two beams effectively generate a time-varying capacitor, the output current of which is given by

$$I = \bar{V}_{dc} \frac{dC}{d\bar{u}} \frac{d\bar{u}}{dt}, \quad (13)$$

where $\bar{V}_{dc}$ is the dc bias voltage of the differential input, $C(\bar{u})$ is the capacitance between the two beams, and $dC/(d\bar{u})$ is the change in the capacitance due to the beams' movement. Since $dC/(d\bar{u})$ is deterministic, $d\bar{u}/dt$ can be measured from the output charging or discharging current of the MEM capacitor formed by the two beams.

A. Mismatch effects in a differential MEMS system

The basic underlying principle of our proposed differential-beam scheme is to take advantage of the symmetry of the system to cancel the effects of external disturbances, which requires that the two beams be as identical as possible. A perfect match in the beam characteristics is not possible in realistic situations as uncertainties, such as manufacturing tolerance, thermal expansion, irregular surface topography, and material property variations, etc., are inevitable.[29] Since the two beams are close to each other, the mismatch caused by thermal effect is insignificant. The main causes of mismatch are various intrinsic structural defects. We analyze two main mismatch mechanisms for our double-beam MEM system.

Mismatch in damping induced by the bottom gap. The typical configuration of a differential MEM system is shown in Fig. 3 where the two symmetrical structures are overlapped and are supported above the substrate by anchors. Except for the damping effect induced by the gap between the two movable structures (denoted as Z_0), the gap between the lower movable structure and the substrate (denoted as Z_b) can also induce squeeze-film damping to the lower structure. Physically, this damping force can be expressed by[22]

$$F_B^A = \frac{\eta w^3}{(Z_b + u_-)^3} \frac{\partial (Z_b + u_-)}{\partial t} = \frac{\eta w^3}{(Z_b + u_-)^3} \frac{\partial u_-}{\partial t}. \quad (14)$$

The force only affects the dynamics of beam $-$ in Eq. (1), which induces viscous force to the beam $-$. Our analysis and computation reveal that this mismatched damping effect

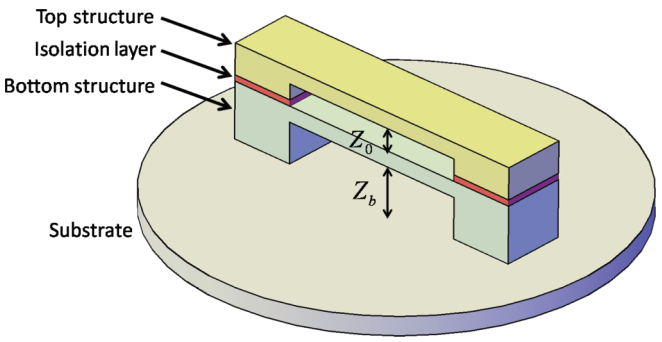

FIG. 3. (Color online) Schematic of the differential electrostatic doubly clamped beams where Z_0 is the gap between the two beams and Z_b is the gap between the lower beam and the bottom electrode.

can deteriorate the perturbation-resisting performance of differential MEM switches.

Mismatch in thickness. In the lateral fabrication process, to control the thickness of the deposited silicon or metal film is difficult. Since, in the differential device shown in Fig. 3, the two movable beams are deposited at different layers, their thicknesses will always have errors with respect to their designed values, leading to mismatches of the differential beams' dynamical properties. Here, the thickness mismatch is defined as

$$\Delta\delta = \frac{\delta_+ - \delta_-}{2}. \tag{15}$$

By considering the two mismatch effects discussed here, the mismatched physical model for the differential device can be modified as

$$\begin{aligned} \rho A_+ \frac{\partial^2 u_+}{\partial t^2} + EI_+ \frac{\partial^4 u_+}{\partial x^4} &= F_+^E + F_+^A + F_+^S, \\ \rho A_- \frac{\partial^2 u_-}{\partial t^2} + EI_- \frac{\partial^4 u_-}{\partial x^4} &= F_-^E + F_-^A + F_B^A + F_-^S, \end{aligned} \tag{16}$$

which will be used below for the performance analysis of a differential MEM resonator.

B. Performance of a differential MEM resonator

The geometrical parameters of the system are as follows: beam width $w = 100\ \mu$m, length $L = 800\ \mu$m, thickness $\delta = 2\ \mu$m, initial gap $Z_0 = 2\ \mu$m, cross-sectional area $A = w \times \delta = 200\ \mu\text{m}^2$, and moment of inertia $I = w\delta^3/12 = 66.67 \times 10^{-24}\ \mu\text{m}^4$. The material parameters of the beams are as follows: Young's modulus $E = 169$ GPa and density $\rho = 2231\ \text{kg/m}^3$. To compensate the difference between the outputs of our system and the conventional SMS system so as to make a fair comparison, we set the air viscosity of our system to be half that of the SMS system. The input voltage should, however, be $\sqrt{2}$ times smaller in our case. Under these settings, the performances of the two types of systems are similar in the absence of any impulsive perturbation.

A basic requirement for a resonator is that the output signal be sinusoidal with the same frequency as that of the input signal (e.g., no harmonics). For the SMS system, we assume it is under room temperature, so the air viscosity is $\eta = \eta_{\text{room}} = 1.82 \times 10^{-5}\ \text{kg/ms}$. The viscosity in our differential MEM system is chosen to be $\eta' = \eta/2 = 0.91 \times 10^{-5}\ \text{kg/ms}$. We

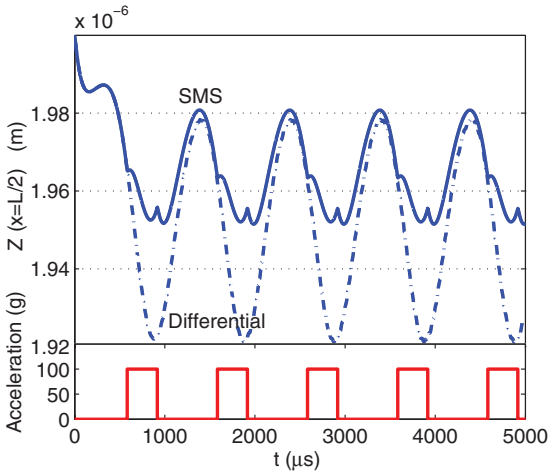

FIG. 4. (Color online) For our differential MEM system and traditional SMS system, comparison of the effects of impulsive perturbation on the device operation as MEM resonators where the desirable output signal is sinusoidal with the same frequency as that of the input signal. The behavior before the arrival of the first impulse is initial transient resulted from the choice of the initial conditions in the simulation.

consider the nonideal case where there is a 5% thickness mismatch effect between the two beams and the bottom gap is set to be $Z_b = 20\ \mu$m. The input voltage signal consists of a dc bias V_{dc} and a small ac component: $V(t) = V_{dc} + V_{ac}\cos(2\pi f t)$, where V_{ac} is the amplitude of the ac driving and f is its frequency. Since the ac signal is small, in the absence of impulsive perturbation, the output of the MEM resonator should be a purely sinusoidal signal of the same frequency. In the presence of such a perturbation, however, the output of the SMS system will typically be distorted.[14] Results from both SMS and our system are shown in Fig. 4 where the voltage amplitudes and the frequency are $V_{dc} = 2$ V, $V_{ac} = 1$ V ($\bar{V}_{dc} = 2/\sqrt{2} = \sqrt{2}$ V and $\bar{V}_{ac} = 1/\sqrt{2}$ V for a differential MEM system), and $f = 1$ KHz. In the simulation, the impulsive perturbation consists of periodic square pulses of magnitude $a = 10^2$ g and duration $T/3$, where $T = 1/f = 1$ ms is the period of the ac input. One can see that, as a result of the perturbation, a strong distortion is present in the output of the SMS system, preventing it from functioning properly as a resonator. However, in our system, the effects of the perturbation on the two symmetrical beams are effectively canceled, and the output is a faithful sinusoidal signal, which is essential for the device to function as a resonator. This is, thus, strong evidence that our differential MEM system can serve as a perturbation-immune resonator.

V. CONCLUSION

To summarize, we have proposed and have investigated the anti-phase synchronization dynamics of a class of microscale systems consisting of two symmetrical electrostatic MEM beams under a differential input voltage. Detailed physical modeling and mathematical analysis indicate the existence of a low-dimensional manifold of differential output, determined by the dynamics of a single electrostatically actuated beam in the absence of any perturbation. Dynamics in the manifold are

immune to external perturbation, especially those of an impulsive nature. Performance in terms of microscale resonators against impulsive perturbation is demonstrated to be superior in our system. Our differential MEM system not only is interesting from the standpoint of basic physics and nonlinear dynamics as it brings important phenomena, such as nonlinear synchronization into microscale systems, but also has tremendous application potential in the design of various kinds of MEM devices that are super-resistant to external disturbances.

We remark that, whereas, synchronization in nonlinear systems has been studied extensively and continues to be an extremely active area of research, the majority of the existing papers focused on systems of coupled low-dimensional oscillators.[2] The importance of synchronization in physically realistic micro- or nanoscale systems has been gradually recognized, and recent papers have suggested that the phenomenon can be exploited for significant applications in nanotechnology.[3–10] Despite these papers, the phenomenon of anti-phase synchronization, where two MEM beams oscillate in completely opposite phase with respect to each other, had not been reported. In terms of basic science, due to the differential system's increased degrees of freedom, by electrostatically driving the system into the nonlinear domain,[16] one effectively creates a paradigm to investigate a variety of complex dynamical behaviors, such as phase synchronization, chaos synchronization, and intermittency in small-scale devices. From an application point of view, complex nonlinear dynamical behaviors, such as anti-phase synchronization studied in this paper, may possess a remarkable degree of robustness against external perturbation. This can be exploited for developing novel MEM systems with superior anti-perturbation/disturbance capabilities.

ACKNOWLEDGMENTS

This work was supported by the NSF under Grant No. EPDT-1101797 and by an ARO STIR Project under the Program of Complex Dynamics and Systems. This work was also supported by the Korea Science and Engineering Foundation WCU Grant No. R32-2009-000-20021-0.

[1] S. H. Strogatz, *Sync: The Emerging Science of Spontaneous Order*, 1st ed. (Hyperion, New York, 2003).
[2] A. Pikovsky, M. Rosenblum, and J. Kurths, *Synchronization: A Universal Concept in Nonlinear Sciences*, 1st ed. (Cambridge University Press, Cambridge, UK, 2001).
[3] M. Zalalutdinov, K. Aubin, M. Pandey, A. Zehnder, R. Rand, H. Craighead, J. Parpia, and B. Houston, Appl. Phys. Lett. **83**, 3281 (2003).
[4] S. Kaka, M. R. Pufall, W. H. Rippard, T. J. Silva, S. E. Russek, and J. A. Katine, Nature (London) **437**, 389 (2005).
[5] F. Mancoff, N. Rizzo, B. Engel, and S. Tehrani, Nature (London) **437**, 393 (2005).
[6] S.-B. Shim, M. Imboden, and P. Mohanty, Science **316**, 95 (2007).
[7] M. Li, H. Tang, and M. Roukes, Nat. Nanotechnol. **2**, 114 (2007).
[8] M. Bagheri, M. Poot, M. Li, W. P. H. Pernice, and H. Tang, Nat. Nanotechnol. **6**, 726 (2011).
[9] C. A. Holmes, C. P. Meaney, and G. J. Milburn, Phys. Rev. E **85**, 066203 (2012).
[10] M. Zhang, G. S. Wiederhecker, S. Manipatruni, A. Barnard, P. McEuen, and M. Lipson, Phys. Rev. Lett. **109**, 233906 (2012).
[11] F. Massel, S. U. Cho, J.-M. Pirkkalainen, P. J. Hakonen, T. T. Heikkilä, and M. A. Sillanpää, Nat. Commun. **3**, 987 (2012).
[12] A. Tomadin, S. Diehl, M. D. Lukin, P. Rabl, and P. Zoller, Phys. Rev. A **86**, 033821 (2012).
[13] L.-Y. Cao and Y.-C. Lai, Phys. Rev. E **58**, 382 (1998).
[14] M. I. Younis, R. Miles, and D. Jordy, J. Micromech. Microeng. **16**, 2463 (2006).
[15] S. W. Yoon, N. Yazdi, N. C. Perkins, and K. Najafi, Sens. Actuators, A **130-131**, 166 (2006).
[16] S. K. De and N. R. Aluru, J. Microelectromech. Syst. **15**, 355 (2006).
[17] M. I. Younis, D. Jordy, and J. M. Pitarresi, J. Microelectromech. Syst. **16**, 628 (2007).
[18] M. W. Weber, EP Patent No. 1,840,508, 2007.
[19] K. Najafi and J. Chae, U.S. Patent No. 6,938,484, 2005; S. Je, F. Rivas, R. Diaz, J. Kwon, J. Kim, B. Bakkaloglu, S. Kiaei, and J. Chae, IEEE Trans. Biomed. Circ. Sys. **3**, 348 (2009).
[20] P. M. Osterberg and S. D. Senturia, J. Microelectromech. Syst. **6**, 107 (1997).
[21] B. McCarthy, G. G. Adams, and N. E. McGruer, J. Microelectromech. Syst. **11**, 276 (2002).
[22] K. Park, Q. Chen, and Y.-C. Lai, Phys. Rev. E **77**, 026210 (2008).
[23] S. K. De and N. R. Aluru, Phys. Rev. B **74**, 144305 (2006).
[24] R. Lifshitz and M. L. Roukes, Phys. Rev. B **61**, 5600 (2000).
[25] G. Rebeiz and J. Muldavin, IEEE Microw. Mag. **2**, 59 (2001).
[26] E. S. Hung and S. D. Senturia, J. Microelectromech. Syst. **8**, 280 (1999).
[27] M. I. Younis, E. M. Abdel-Rahman, and A. Nayfeh, J. Microelectromech. Syst. **12**, 672 (2003).
[28] F. D. Frank, D. Bannon III, J. R. John, R. Clark, C. T. C. Clark, and T. C. Nguyen, J. Solid State Circuits **35**, 512 (2000).
[29] G. T. A. Kovacs, *Micromachined Transducers Sourcebook* (McGraw-Hill, New York, 1998).